Microscopic investigation on the existence of transverse wobbling under the effect of rotational alignment: The ^{136}Nd case

Fang-Qi Chen [1] and C. M. Petrache [2]

[1]*School of Physical Science and Technology, Northwestern Polytechnical University, Xi'an 710129, China*
[2]*Centre de Sciences Nucléaires et Sciences de la Matière, CNRS/IN2P3, Université Paris-Saclay, Bâtiment 104-108, 91405 Orsay, France*

The even- and odd-spin two-quasiparticle yrast bands in ^{136}Nd are investigated with the triaxial projected shell model, focusing on the possible interpretation as transverse wobbling. With the experimental observables reproduced reasonably, the conditions under which the wobbling approximation is valid are examined via the angular momentum geometry and the configuration components extracted from the microscopic wave functions. The impact of the rotational alignment of the quasiparticles on the scenario of transverse wobbling is emphasized. It turns out that the $n = 0$ band of the wobbling candidate is more affected than the $n = 1$ one, which tends to go against the decreasing trend of the wobbling energy expected in the transverse case.

I. INTRODUCTION

The concept of wobbling motion is originally proposed by Bohr and Mottelson [1] for a triaxial rotor as a harmonic excitation based on the uniform rotation around the intrinsic axis with the largest moment of inertia (MoI). The harmonicity is achieved when the angular momentum component on the axis with the largest MoI is almost as large as the total angular momentum. In this case a bosonlike commutation rule applies approximately between the raising and lowering operators of the angular momentum component involved (see Sec. 4-5e in Ref. [1]), allowing the introduction of a wobbling phonon. The phonon describes harmonic precession oscillations of the angular momentum vector around the principle axis with the largest MoI, giving rise to characteristic equally spaced energies and quantized transition probabilities. The harmonic condition is better satisfied with larger amount of total angular momentum, so the wobbling spectra are usually expected in the high-spin region.

Apart from the phenomenological triaxial rotor model, the wobbling motion has also been described in microscopic frameworks based on the random-phase approximation (RPA)-like methods. The first attempt to describe the wobbling motion in an RPA framework was proposed by Marshalek in Ref. [2], based on the self-consistent cranking (SCC) solution. The method called "SCC + RPA" is then improved by taking care of the rotational invariance of the Hamiltonian [3]. The rotational invariance is also taken into account by the work of Mikhalov and Janssen [4,5], but treated in a different way. The different treatments of rotational invariance are later proved to be equivalent in Ref. [6], in which the SCC + RPA framework is derived by the time-dependent Hartree-Bogoliubov method, and the wobbling effect is reflected by the time dependence of either deformation or angular velocity.

The wobbling motion for a single rotor was later called "simple wobbling," in order to distinguish it from the wobbling modes with quasiparticle(s) involved [7]. The latter ones are further distinguished according to the coupling scheme between the quasiparticle(s) and the rotor. When the angular momentum of the quasiparticle(s) is perpendicular to the principle axis favored by collective rotation, the transverse wobbling is expected. In this case the precession happens around the orientation of the quasiparticle angular momentum, rather than the favored axis of collective rotation. With sufficient quasiparticle angular momentum the transverse wobbling can take place at the bandhead and is therefore easier to observe. The longitudinal wobbling, on the other hand, is expected when the angular momentum of the quasiparticle(s) aligns with the axis favored by collective rotation, and the precession, of course, happens around the orientation of both.

The mechanism of transverse wobbling was investigated theoretically long before the invention of its name, by both the particle-rotor model (PRM) and the RPA. Based on the particlelike quasiparticle configurations arising from a cranked mean field, it was shown that the RPA MoI is largest for the short axis, rather than the intermediate axis in the simple rotor case. Such an MoI distribution leads to the wobbling motion around the short axis [8], which is in fact the transverse wobbling. The investigations based on the particle-rotor model followed two branches. The first one [9] involved the so-called γ-inverted MoI with the γ dependence of the irrotational MoI changed by hand, so that the one of the short-axis can become largest (similar to the RPA case). However, such an attempt eventually leads to the longitudinal wobbling rather than to the transverse one. The other one, reported in Refs. [7,10], proceeds the PRM framework by distinguishing the angular momentum contributed by the rotor and the valence particle. A rotorlike Hamiltonian can be obtained in this way,

with the effective MoI following the RPA distribution, and consequently leads to the transverse wobbling solution. As is pointed out in Ref. [10], both the RPA and the PRM descriptions share the key point that the MoI distribution (and consequently, the spin orientation) can be changed substantially by the existence of the valence (quasi)particle. The decreasing of the wobbling energy against spin or rotational frequency is first noted in Ref. [10] and then in Ref. [7], which is later known as the "hallmark" of transverse wobbling.

The only candidates for a simple wobbler observed experimentally up to now are ^{112}Ru [11] and ^{114}Pd [12], in which the so-called "γ bands" are interpreted as a combination of $n = 1$ (odd-spin) and $n = 2$ (even-spin) wobbling excitations as the odd-even staggering pattern agrees with the expectation of rigid triaxiality [13]. However, these interpretations are not confirmed solidly yet, due to the lack of transition probability measurements. On the other hand, the wobbling motion with high-j quasiparticle(s) involved have been suggested in various mass regions. The wobbling bands reported in ^{161,163,165,167}Lu [14–18] and ^{167}Ta [19] were interpreted by Hamamoto and Hagemann [9,20] as arising from configurations with a high-j aligned particle, which is equivalent to the longitudinal wobbling. Some of them are later reinterpreted as transverse wobbling [7], according to the decreasing behavior of the wobbling energy. In recent years, the transverse wobbling candidates have also been reported in ^{105}Pd [21], ^{135}Pr [22,23], and ^{183}Au [24]. The only example of transverse wobbling in an even-even nucleus is the $\pi(h_{11/2})^2$ bands in ^{130}Ba [25–27]. It was suggested as the best-known case for transverse wobbling [26], probably due to its larger amount of quasiparticle angular momentum, contributed by two quasiparticles instead of one. The experimental fingerprints of longitudinal wobbling were reported in ^{133}La [28], ^{187}Au [29], and ^{127}Xe [30]. However, one has to bear in mind that some of these suggested wobblers are still under debate from both theoretical and experimental points of view [31–34].

As a solution of the RPA, the stability of the transverse wobbling might be questioned. It is demonstrated in Ref. [35] that the "softening" of the transverse wobbling closely relates to the shifting of the minimum of the total Ruthian surface, calculated by three-dimensional cranking, from the short axis to a tilted planar orientation. The stability of the transverse wobbling can also be examined within the PRM framework. In fact, the existence of transverse wobbling has been questioned recently by a quantitative examination of the harmonic condition given in Refs. [1] and [7], in terms of the MoI of the three intrinsic principle axes [36]. The result of the examinations, carried out for various choices of MoI parameters used in actual particle-rotor model calculations, suggested that the harmonic approximation condition demanded for transverse wobbling is hardly satisfied. The investigation highlights the gap between the particle-rotor model calculations, which are used to reproduce the experimental data, and the wobbling approximation, which is used to interpret them. Such a gap is sometimes forgotten in the theoretical discussions of the transverse wobbling candidates.

However, the condition function examined in the above investigation [36] may be worth a second consideration, as it

can be connected to the angular momentum condition for the boson approximation only if the harmonicity is perfectly realized. With a deviation from the harmonic limit the meaning of the function is not very clear. Moreover, the function for the transverse wobbling in Ref. [36] is in fact identical to that for the simple wobbling, due to the correspondence between their Hamiltonians (see Eqs. (11) and (13) in Ref. [7]) which arises under the frozen alignment approximation. The frozen alignment assumes that the single-particle angular momentum always align to the short axis (s axis). Therefore, the effect of rotational alignment, which drives the single-particle angular momentum to the intermediate axis (i axis) for triaxial nuclei, is not discussed in Ref. [36]. On the other hand, in Ref. [36] only one-quasiparticle bands in odd-mass nuclei are discussed. With the recent observation in ^{130}Ba, the existence of transverse wobbling in two-quasiparticle bands of even-even nuclei also deserves a discussion, which, as mentioned above, might be more stable than those in the odd-mass cases.

In this work we present an investigation of the transverse wobbling candidate, i.e., band L3 in ^{136}Nd [37], having the same two-quasiparticle configuration as that in ^{130}Ba, with the triaxial projected shell model. In such a microscopic framework the input of the MoI as free parameters as in the particle-rotor model calculations are avoided, and the harmonic condition is examined in its original form, i.e., in terms of angular momentum geometry. The alignment tendency of the quasiparticles is also taken into account, with its effect carefully discussed. The model framework is briefly outlined in Sec. II. In Sec. III, the results of the calculation are presented, and the quantities related to the wobbling scenario are analyzed. A short summary is given in Sec. IV.

II. THEORETICAL FRAMEWORK

The present model starts from the schematic pairing-plus-quadrupole Hamiltonian [38]

$$\hat{H} = \hat{H}_0 - \frac{\chi}{2} \sum_\mu \hat{Q}_\mu^\dagger \hat{Q}_\mu - G_M \hat{P}^\dagger \hat{P} - G_Q \sum_\mu \hat{P}_\mu^\dagger \hat{P}_\mu, \quad (1)$$

in which $\hat{H}_0$ represents the spherical single-particle Hamiltonian and the following three terms are the quadrupole-quadrupole interaction, the monopole pairing, and the quadrupole pairing, respectively. The self-consistent minimum $|\Phi_0\rangle$ is found for the above Hamiltonian by a Hartree-Fock-Bogoliubov iteration, together with a set of quasiparticle orbitals i defined by

$$\beta_i |\Phi_0\rangle = 0 \quad \text{for } \forall i, \quad (2)$$

in which β_i represents the quasiparticle annihilation operator. The intrinsic configuration $|\Phi_\kappa\rangle$ is taken from the set

$$|\Phi_\kappa\rangle \in \{|\Phi_0\rangle, \beta_i^\dagger \beta_j^\dagger |\Phi_0\rangle\}, \quad (3)$$

with i and j taken from the $\pi h_{11/2}$ subshell, in accordance with the $\pi(h_{11/2})^2$ configuration assigned to the wobbling candidates under consideration. Each intrinsic configuration $|\Phi_\kappa\rangle$ is projected onto good angular momentum as well as particle numbers. The Hamiltonian is then diagonalized with

the projected basis

$$\{\hat{P}^I_{MK}\hat{P}^N\hat{P}^Z|\Phi_\kappa\rangle\}, \qquad (4)$$

leading to the Hill-Wheeler equation

$$\sum_{K'\kappa'}\left[\mathcal{H}^I_{KK'}(\kappa,\kappa')-E^{I\sigma}\mathcal{N}^I_{KK'}(\kappa,\kappa')\right]f^{I\sigma}_{K'\kappa'}=0, \qquad (5)$$

with the kernels

$$\mathcal{H}^I_{KK'}(\kappa,\kappa') \equiv \langle\Phi_\kappa|\hat{H}\hat{P}^I_{KK'}\hat{P}^N\hat{P}^Z|\Phi_{\kappa'}\rangle,$$
$$\mathcal{N}^I_{KK'}(\kappa,\kappa') \equiv \langle\Phi_\kappa|\hat{P}^I_{KK'}\hat{P}^N\hat{P}^Z|\Phi_{\kappa'}\rangle, \qquad (6)$$

calculated using the algorithm in Refs. [39,40]. The eigenvalues $E^{I\sigma}$ can be compared directly to the experimental spectra, and the wave function

$$|\Psi^{I\sigma}\rangle = \sum_{K\kappa} f^{I\sigma}_{K\kappa}\hat{P}^I_{MK}\hat{P}^N\hat{P}^Z|\Phi_\kappa\rangle \qquad (7)$$

with good angular momentum allows a straightforward calculation of the reduced transition probabilities. For a detailed description of the model, one can refer to Refs. [41,42].

Apart from the observables, the quantities in terms of which the wobbling motion is defined are also important for the following discussion, including the orientation of the angular momentum vector in the intrinsic frame (its probability distribution, to be exact), the distribution width of the largest component of the angular momentum, the configuration components, etc. Such quantities are in fact the probability distributions of the arguments involved in the wave functions, like Ω (involved in the angular momentum projector $\hat{P}^I_{MK}$), K, or κ. Due to the nonorthogonality of the projected basis (4), the probability amplitudes of the arguments are not given directly by their corresponding coefficients, but by a transformation of them called the collective wave functions [38], which can be written in general as

$$g^{I\sigma}(\rho) = \sum_\rho \Pi^{1/2}(\rho,\rho')F^{I\sigma}_{\rho'}, \qquad (8)$$

with ρ representing the arguments under discussion and $\Pi^{1/2}(\rho,\rho')$ representing the square root of the corresponding kernel $\Pi(\rho,\rho')$:

$$\sum_{\rho'}\Pi^{1/2}(\rho,\rho')\Pi^{1/2}(\rho',\rho'') = \Pi(\rho,\rho'') \equiv \langle\tilde{\Phi}(\rho)|\tilde{\Phi}(\rho'')\rangle. \qquad (9)$$

For example, the probability distribution of the angular momentum orientation can be obtained by calculating the collective wave function $g^{I\sigma}(\Omega,\kappa)$ and then summing over κ, which means $\rho = \{\Omega,\kappa\}$ and $|\tilde{\Phi}(\rho)\rangle = \hat{R}(\Omega)|\Phi_\kappa\rangle$, while the probability distribution of the angular momentum component K can be obtained from the collective wave function $g^{I\sigma}(K,\kappa)$, so there are $\rho = \{K,\kappa\}$ and $|\tilde{\Phi}(\rho)\rangle = \hat{P}^I_{MK}|\Phi_\kappa\rangle$. The explicit expressions of the above probability distributions, called the "azimuthal plot" and the "K plot," respectively, can be found in Ref. [43]. The weight of the configuration κ, of course, also comes from $g^{I\sigma}(K,\kappa)$ and its explicit expression is given in Ref. [44]. Similar plots can be calculated in the framework of the particle-rotor model [26,45,46] as well.
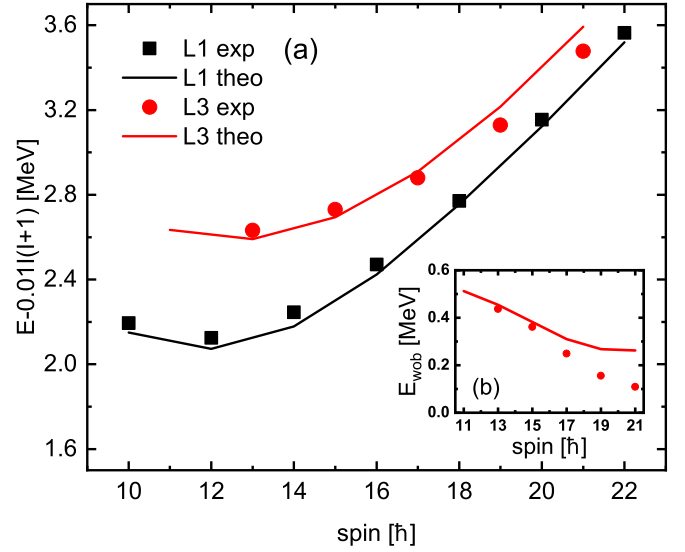

FIG. 1. (a) Calculated energies (minus a common rigid-rotor reference) of the even- and odd-spin yrast bands in ^{136}Nd, in comparison with the experimental data (see bands L1 and L3 in Ref. [37]). (b) Wobbling energies (see the text) obtained by the calculation compared with the experimental results from bands L1 ($n=0$) and L3 ($n=1$).

In the present calculation the neutron and proton major shells with $N = 3$, 4, and 5 are considered as the model space. The single-particle Hamiltonian $\hat{H}_0$ is the Nilsson Hamiltonian at zero deformation, with its parameters κ and μ modified based on the values given in Ref. [47]. The values of κ and μ for the neutron shell $N = 5$ are multiplied by a factor of 0.8, while those for the proton shells $N = 4$ and $N = 5$ are multiplied by 0.6 and 0.9, respectively. The strengths for the quadrupole-quadrupole interactions are $\chi_{\tau\tau'} = \chi\alpha_\tau\alpha_{\tau'}$, with $\alpha_\pi = (2Z/A)^{1/3}$ and $\alpha_\nu = (2N/A)^{1/3}$ for $\tau(\tau')$ being proton or neutron, respectively. The choice of $\chi = 70A^{-1.4}/b^4$ MeV (where $b = A^{1/6}$ is the oscillation length) is taken from Ref. [48], and the reducing factor multiplied by the matrix elements of the quadrupole operator $\hat{Q}_\mu$ between the orbitals from the $N = 5$ shell, suggested in Ref. [48], is also adopted. The strengths of the monopole pairing are $G_M = 0.17$ MeV for neutrons and $G_M = 0.12$ MeV for protons, and those of the quadrupole pairing are $G_Q = 0.16G_M$. The self-consistent minimum is found with deformations $\beta \approx 0.17$ and $\gamma \approx 28°$, being comparable with the result of the Hartree-Fock-Bogoliubov (HFB) calculation using the D1S Gogny interaction [49]. The significant triaxiality also fulfills the conditions required for the presence of wobbling motion.

III. RESULTS AND DISCUSSIONS

The calculated energy spectra of the transverse wobbling candidates with the configuration $\pi(h_{11/2})^2$ in ^{136}Nd are shown in Fig. 1 and are compared with the experimental data (labeled as bands L1 and L3). Good agreement is achieved for band L1 within the whole spin region. For band L3 the levels near the bandhead are more or less well reproduced, while those at higher spins are overestimated, similar to the
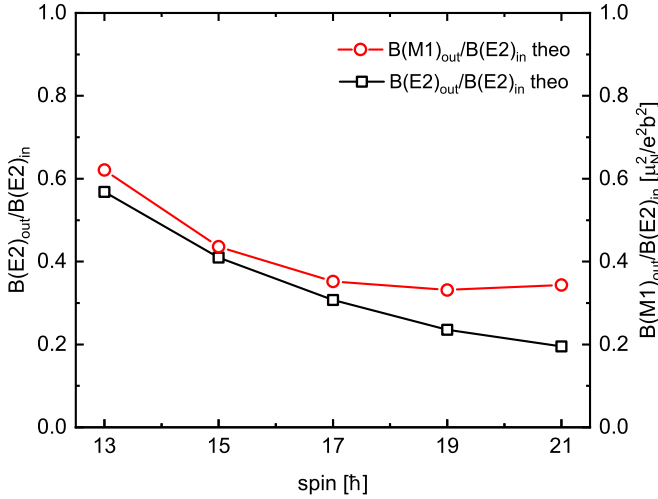
FIG. 2. Calculated ratios between the interband [$B(E2/M1)_{\rm out} \equiv B(E2/M1, I \to I-1)$ from band L3 to band L1] and the intraband [$B(E2)_{\rm in} \equiv B(E2, I \to I-2)$ along band L3] transition probabilities.

case in ^{130}Ba with the same model [27]. It is expected that the reproduction can be improved by enlarging the model space with more quasiparticle configurations. The wobbling energy, obtained by

$$E_{\rm wob} = E(I, n = 1) - [E(I-1, n = 0) \\ + E(I+1, n = 0)]/2, \qquad (10)$$

is given in the inset of the same figure. Its down-sloping behavior against spin, often regarded as one of the hallmarks of transverse wobbling, is qualitatively reproduced. The overestimation of $E_{\rm wob}$ for higher spins is due to that of band L3. It is worth mentioning that, apart from the two bands shown in Fig. 1, the bands starting from low spin, i.e., the ground-state band and the γ-band in Ref. [37], can be also well reproduced with the same set of parameters.

The calculated ratios between the interband and intraband transition probabilities $B(E2)_{\rm out}/B(E2)_{\rm in}$ and $B(M1)_{\rm out}/B(E2)_{\rm in}$ are shown in Fig. 2, with no experimental measurement up to now. The overall magnitude of the calculated values are comparable to those of the wobbling bands in ^{130}Ba [26], supporting the possible interpretation of transverse wobbling. The decreasing behavior of the calculated values is in qualitative agreement with the analytical expressions obtained with the wobbling approximation [1,7].

As most of the existing data for the observables are reasonably reproduced and basically compatible with the expectation of transverse wobbling, it is worthwhile to have a look at the orientation of the angular momentum in the intrinsic frame, in terms of which the wobbling motion is proposed. The probability density distribution profiles for the tilted angles (θ, ϕ) of the angular momentum vector with respect to the three principal axes (i.e., the so-called "azimuthal plots" [43]) are shown in Fig. 3 for the wobbling candidates.

The distribution for the bandhead of L1 is centered around the peak at $(\theta = 90°, \phi = 0°)$, suggesting the firm

alignment of the angular momentum along the s axis, as expected for a particlelike configuration $\pi(h_{11/2})^2$ (see the following). As spin increases, the collective rotation develops, with the orientation of its angular momentum determined by the competition between the Coriolis effect and the distribution of the MoI among the three principal axes. The former one prefers the alignment of the collective angular momentum to the s axis, while the latter one favors the collective rotation around the i axis. It seems that the Coriolis effect dominates with moderate spin, as the peak at $(\theta = 90°, \phi = 0°)$ remains until $I = 16\hbar$. However, the angular momentum feels increasing attraction from the i axis, as the distribution is more and more stretched along the s-i plane. Finally at $I = 18$ the abovementioned peak splits into two, with both of them moving towards the i axis with further increasing spin. The Coriolis effect in this case, however, tends to drive the quasiparticle angular momentum to the i axis, as is discussed in the following.

The transverse wobbling can take place when the angular momentum of the yrast band (L1) aligns along the s axis. It can be inferred from Fig. 3 that the distribution for the bandhead of L3 revolves around the node at $(\theta = 90°, \phi = 0°)$, in coincidence with the wobbling motion around the s axis. The revolving behavior continues to moderate spin, with the two peaks in the i-s plane growing sharper and sharper as spin increases, due to the development of collective rotation around the i axis. On the other hand, the distribution in the s-l plane becomes less and less and fades away at sufficiently large spin, as the result of the smallest MoI of the l axis. At its disappearance the revolving structure at the bandhead no longer exists and the probable transverse wobbling collapses. It is shown that the overall evolution of the tilted-angle distributions for bands L1 and L3 is in qualitative agreement with the transverse wobbling scenario close to the bandheads, and a quantitative examination for the validity of the wobbling approximation is therefore necessary.

The concept of transverse wobbling is proposed assuming that the single-particle angular momentum aligns firmly with the s axis [7]. With this assumption the particle-rotor Hamiltonian can be mapped [7] to the simple rotor Hamiltonian in Ref. [1]. The bosonlike commutation rule there (see Eq. (4-296) in Ref. [1]) is thus transformed as

$$[\hat{I}_-, \hat{I}_+] = 2\hat{I}_s \approx 2I, \quad \hat{I}_\pm = \hat{I}_l \pm i\hat{I}_i, \qquad (11)$$

which means that the states under discussion should be approximate eigenstates of the operator $\hat{I}_s$ with the eigenvalue I:

$$\hat{I}_s|\Psi^{I\sigma}\rangle \approx I|\Psi^{I\sigma}\rangle. \qquad (12)$$

The distribution of the angular momentum component (i.e., the so-called K plot in Ref. [43]) on the s axis shown in Fig. 4 provides the probability of $I_s = I$ and therefore reflects the validity of the boson approximation (11).

The distribution for I_s at the bandhead of L1 shows a sharp peak at $I_s = I$, with the height (~ 0.6) more or less comparable to the corresponding result of the known example of transverse wobbling, i.e., band S1 in ^{130}Ba [27]. It is therefore suggested that the boson approximation (11) is satisfied to a similar extent as in ^{130}Ba near the bandhead. As
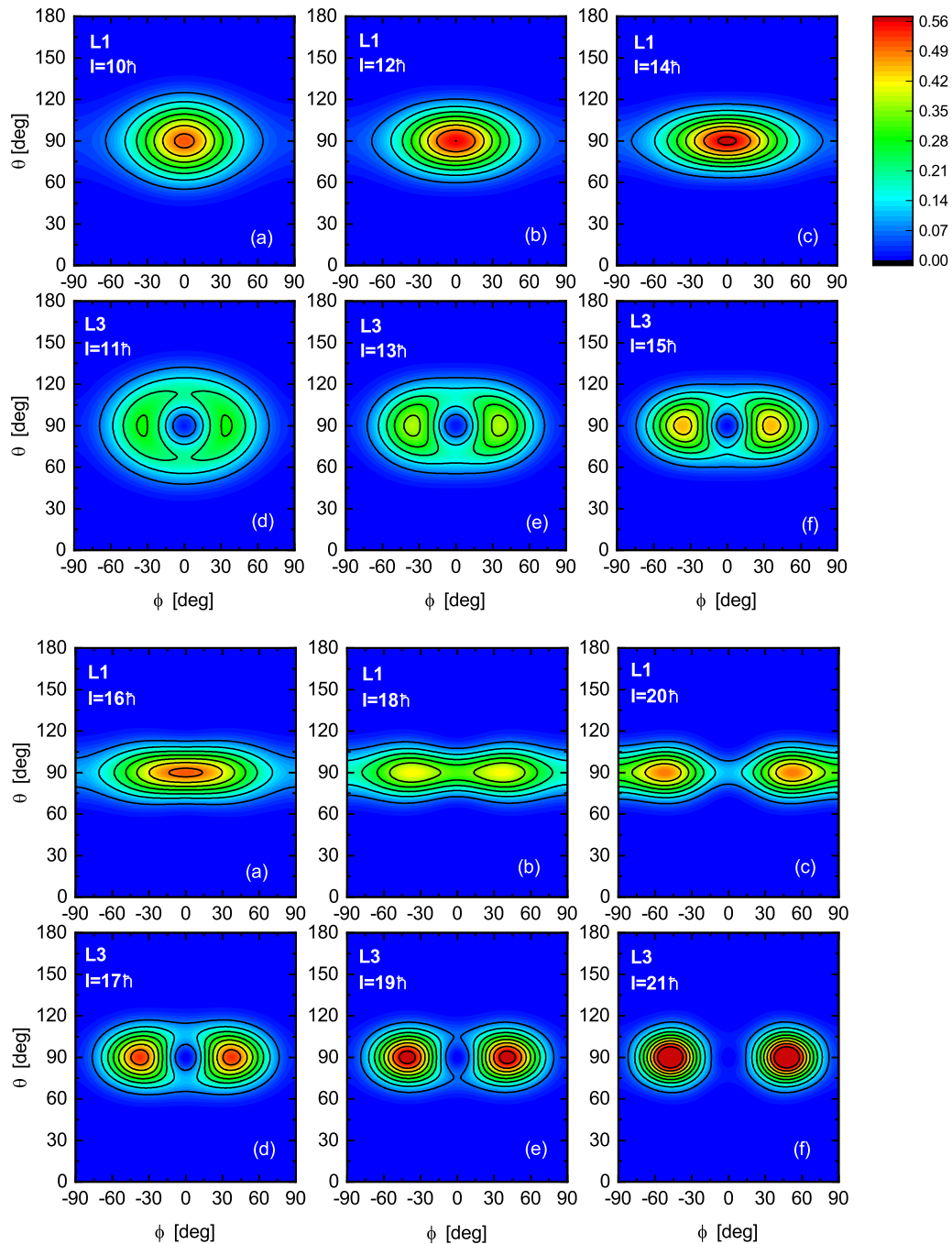
FIG. 3. Probability distribution profiles for the tilted angles (θ, ϕ) of the angular momentum vector $\vec{J}$ with respect to the three principle axes of the intrinsic frame for bands L1 and L3 in ^{136}Nd. The polar angle θ represents the angle between $\vec{J}$ and the long axis (l axis), while the azimuthal angle ϕ represents the angle between the projection of $\vec{J}$ on the short-intermediate plane and the short axis (s axis). Note that the definition of ϕ here in coincidence with Ref. [26] is different from the definitions in Refs. [27,43].

spin increases, the peak at $I_s = I$ remains until $I = 18\hbar$ for band L1, with a decreasing height indicating the erosion of the boson approximation (11) and therefore of the transverse wobbling. A similar decreasing trend can also be found in ^{130}Ba, but at a smaller rate [27]. For example, at $I = 16\hbar$ the height of the $I_s = I$ peak for the band L1 of ^{136}Nd is about 0.4, while that for the S1 band of ^{130}Ba is more than 0.5. It is suggested that the transverse wobbling pattern for the $n = 0$ band in ^{136}Nd is less stable than that in ^{130}Ba. This can

also be confirmed qualitatively by a comparison between the orientation distributions of the angular momentum vector of the two nuclei. For ^{136}Nd the most probable orientation for the $n = 0$ band deviates from the s axis at $I = 18\hbar$, while for ^{130}Ba it remains at the s axis till $I = 22\hbar$. The $I_s = I$ peak in the I_s distribution for band L1 disappears at $I_s = 20\hbar$, showing the complete collapse of the boson picture.

The evolution of the I_s distribution for band L3 in ^{136}Nd provides information similar to that of L1. The peak at
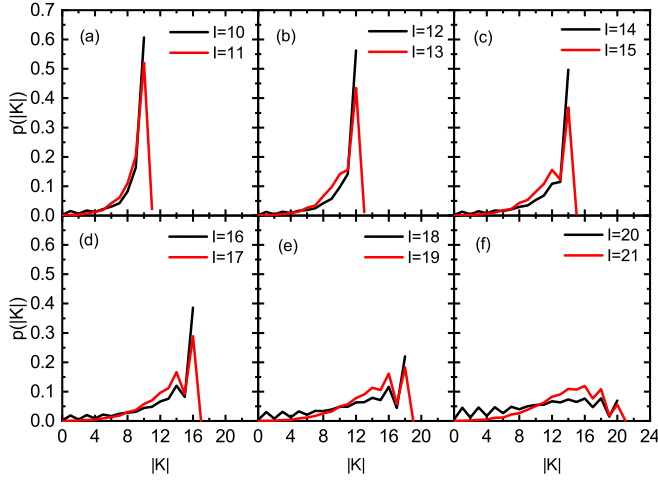
FIG. 4. Probability distributions of the angular momentum component on the short axis, calculated for bands L1 and L3 in ^{136}Nd.
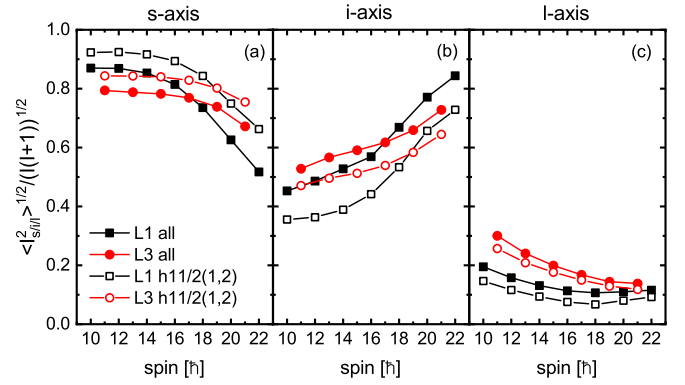

FIG. 5. The ratios between the root mean squares of the angular momentum components $\langle \hat{I}^2_{s/i/l} \rangle^{1/2}$ and that of the total angular momenta $\langle \hat{I}^2 \rangle^{1/2}$, calculated for the short (s), intermediate (i), and long (l) axes, respectively, for bands L1 and L3 in ^{136}Nd. The solid symbols represent results calculated with configuration mixing within the $\pi h_{11/2}$ subshell, while the open symbols represent those calculated with the fixed configuration $\pi h_{11/2}(1, 2)$ composed of the lowest two Nilsson orbitals in the $h_{11/2}$ subshell.

$I_s = I - 1$ shown in the distribution for the bandhead is consistent with the expectation of one-phonon transverse wobbling, and its decreasing height with spin, again, reflects the erosion of the phonon structure. The complete disappearance of the $I_s = I - 1$ peak at $I = 21\hbar$ also coincides with the collapse of transverse wobbling suggested by the above discussions for band L1. However, by a careful inspection one may find that the decreasing rate of the height of the $I_s = I - 1$ peak in band L3 is more or less comparable to its corresponding band in the ^{130}Ba case, at least for the moderate spin range $I \leqslant 17\hbar$ [27]. In fact, the height of the peaks in both cases decrease from ~ 0.5 to ~ 0.3, when the spin goes from $I = 11$ to $17\hbar$. Therefore, it seems that the stability of the transverse wobbling for the $n = 1$ band in ^{136}Nd is comparable to that in ^{130}Ba. One may be confused by the result that a one-phonon excitation built upon a zero-phonon state that is *less* stable than that in ^{130}Ba can have a stability *comparable* to its corresponding band in ^{130}Ba. A possible explanation for this is provided in the later discussion.

The condition of transverse wobbling can also be expressed as [7]

$$\langle \hat{I}^2_i + \hat{I}^2_l \rangle \ll \langle \hat{I}^2_s \rangle, \tag{13}$$

which leads to the criteria $f(n, I) \ll 1$, written in terms of the MoI, used in Ref. [36]. In the present model framework the MoIs around the three principle axes are not given explicitly, but the above equation (13) can be examined directly by calculating the root-mean-square angular momentum components on the three principal axes. The calculated ratios $\langle \hat{I}^2_{s/i/l} \rangle^{1/2}/\langle \hat{I}^2 \rangle^{1/2}$ are shown in Fig. 5 by the solid symbols for bands L1 and L3. It is shown that the ratio $\langle \hat{I}^2_s \rangle^{1/2}/\langle \hat{I}^2 \rangle^{1/2}$ reaches about 90% (80%) for bandheads of band L1 (L3), supporting the approximate realization for the transverse wobbling. However, the ratios $\langle \hat{I}^2_i \rangle^{1/2}/\langle \hat{I}^2 \rangle^{1/2}$ reaching around 50% in both bands remind one of the existing deviation from the ideal wobbling scenario. The decrease of $\langle \hat{I}^2_s \rangle^{1/2}$ with spin is accompanied by the increase of $\langle \hat{I}^2_i \rangle^{1/2}$, both suggesting the erosion of the wobbling structure. It is noted that the changing slopes of $\langle \hat{I}^2_s \rangle^{1/2}$ and $\langle \hat{I}^2_i \rangle^{1/2}$ for band L3 are smaller than those

for band L1, leading to the crossings at around $I = 16\hbar$–$18\hbar$ between the curves of the two bands. The result with $\langle \hat{I}^2_s \rangle^{1/2}_{\text{L3}} > \langle \hat{I}^2_s \rangle^{1/2}_{\text{L1}}$ after the crossing is no longer compatible with the expectation for transverse wobbling. For sufficiently large spin there is $\langle \hat{I}^2_i \rangle^{1/2}/\langle \hat{I}^2 \rangle^{1/2} \approx 80\%$, indicating a possible onset of longitudinal wobbling around the i axis, as mentioned in Ref. [7]. The value of $\langle \hat{I}^2_s \rangle^{1/2}/\langle \hat{I}^2 \rangle^{1/2}$ for band L3 smaller than that for L1 before the crossing suggests a better transverse wobbling condition for $n = 0$ than for $n = 1$, in agreement with Ref. [36]. The smaller $\langle \hat{I}^2_i \rangle^{1/2}/\langle \hat{I}^2 \rangle^{1/2}$ for band L3 after the crossing similarly indicates the longitudinal wobbling will also be better defined for the $n = 0$ case. Finally, the values of $\langle \hat{I}^2_l \rangle^{1/2}/\langle \hat{I}^2 \rangle^{1/2}$ keep small and decrease with spin, as a result of the s-axis-aligned quasiparticle angular momentum and the smallest MoI for the l axis.

The angular momentum geometry revealed in the above discussion concludes that the transverse wobbling scenario is more or less valid at the bandhead of the bands L1 and L3 in ^{136}Nd. As spin increases, the wobbling pattern gets destructed and finally disappears around $I = 18\hbar$. The reason for its erosion is twofold. First, the rotational angular momentum converts from the s axis to the i axis due to its large MoI, as discussed above. Such an effect leads to the down-sloping wobbling energy against spin given in Ref. [7], which was later recognized as the hallmark of the transverse wobbling. The second reason for the wobbling erosion is induced by the first one: the quasiparticle angular momentum tends to align along the i axis, instead of the s axis, as the rotational angular momentum converts. Such an effect is realized by configuration mixing in the present model. The destruction of the wobbling scenario by configuration mixing can be quickly seen from the plots with open symbols in Fig. 5, calculated with the fixed configuration $\pi h_{11/2}(1, 2)$ composed by the lowest two orbitals in the $h_{11/2}$ subshell. Comparing with the filled symbol results discussed above, one finds that the transverse wobbling condition (13) is better satisfied at the
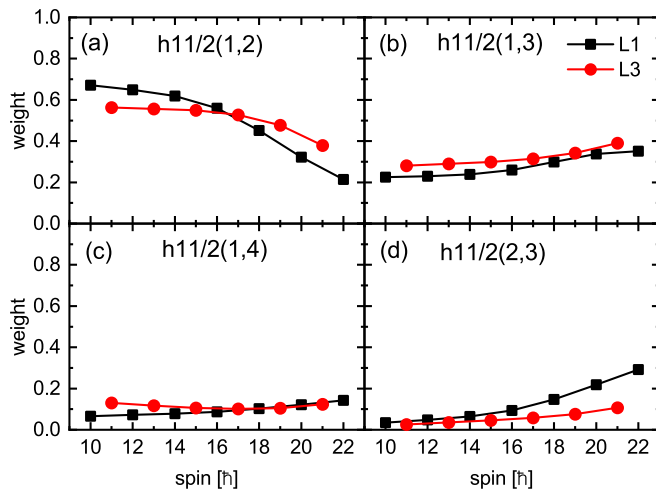
FIG. 6. The weight of the $\pi(h_{11/2})^2$ configurations included in the present calculation, plotted for bands L1 and L3 in ^{136}Nd as functions of spin. The notation (i, j) denotes the two-quasiparticle configuration composed by the ith and the jth Nilsson orbitals in the $\pi h_{11/2}$ subshell (counted from the lowest one).

FIG. 7. The band diagrams of the configurations $h_{11/2}(1, 2)$ and $h_{11/2}(2, 3)$, for both even and odd spins.

bandhead of both bands, and the collapse of wobbling reflected by the crossings of bands L1 and L3 is postponed. The configuration mixing is not taken into account in the description of transverse wobbling under the assumption of frozen alignment [7], as well as the later investigation on its existence [36]. Although it is embedded in the model frameworks of theoretical investigations on the wobbling bands in ^{130}Ba [26,27], its effect on the wobbling picture is not discussed in detail. Therefore, a detailed study of the configuration mixing and, in particular, the quasiparticle alignment in the transverse wobbling bands in ^{136}Nd will be interesting. Here one should note that the phrase "quasiparticle alignment" here means the rotational alignment along the axis with the largest MoI (i axis) due to the developed collective rotation, which should be distinguished from the one in the RPA works such as Ref. [8]. In the context of Ref. [8] the word "alignment" means the quasiparticle excitation with its angular momentum along the s axis. The former tends to destroy the transverse wobbling that the latter leads to.

The weights of the four dominating $\pi(h_{11/2})^2$ configurations in the bands L1 and L3 are shown in Fig. 6 as functions of spin. The particlelike configuration with orbitals at the bottom of the $h_{11/2}$ subshell, i.e., $h_{11/2}(1, 2)$, is found to be dominant near the bandhead, consistent with the frozen alignment assumed for transverse wobbling [7]. As spin increases, the configuration $h_{11/2}(1, 2)$ tends to be replaced by other ones with their orbitals lying closer to the middle of the $h_{11/2}$ sub-shell, showing the alignment of the quasiparticle angular momentum. It is noted that the weight of $h_{11/2}(1, 2)$ decreases with a larger slope in band L1 than in band L3. Correspondingly, the weight of $h_{11/2}(2, 3)$, with its angular momentum closer to the i axis, increases more quickly for band L1. This suggests that the $n = 0$ band is more influenced than the $n = 1$ band by the quasiparticle alignment.

The different extent of influence from the quasiparticle alignment found in bands L1 and L3 provides a possible
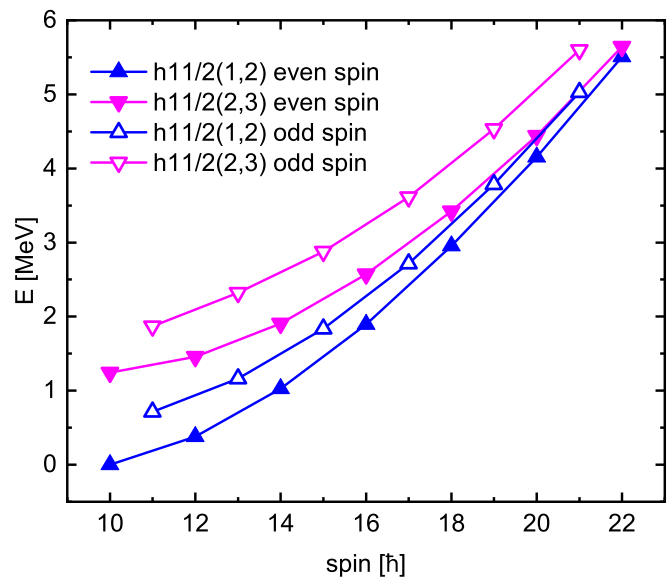
explanation for the comparable stability of the $n = 1$ bands in ^{136}Nd and ^{130}Ba, even though the $n = 0$ band is less stable in ^{136}Nd than in ^{130}Ba. Compared with ^{130}Ba, ^{136}Nd is less deformed and has thus a stronger tendency of quasiparticle alignment. The transverse wobbling in the $n = 0$ band, being more affected by the alignment process, is likely to be less stable in ^{136}Nd than in ^{130}Ba. On the other hand, the $n = 1$ band, which is less sensitive to the quasiparticle alignment, is likely to show comparable stability in the two cases. In other words, the different stability of the transverse wobbling in ^{136}Nd and ^{130}Ba can be explained to a certain extent by the different tendency of the quasiparticle alignment to the i axis.

A possible interpretation for the different extents of the quasiparticle alignment shown in the $n = 0$ and $n = 1$ bands may be given by the decreasing behavior of the transverse wobbling energy as a function of spin. This can be inferred from Fig. 7, which shows the band diagrams of configurations $h_{11/2}(1, 2)$ and $h_{11/2}(2, 3)$, which exhibit relatively large discrepancies between bands L1 and L3 (see Fig. 6). The band diagrams shown in Fig. 7 are the lowest energies obtained by the diagonalization of the Hamiltonian within spaces spanned by projecting the considered configuration onto the specified spin I and all possible angular momentum components K. It is shown that the odd-even staggering for the $h_{11/2}(1, 2)$ configuration, which is exactly the E_{wob} in Eq. (10) neglecting the configuration mixing, decreases substantially with spin, while that for $h_{11/2}(2, 3)$ keeps more or less constant due to its less particlelike character. As a result, the energy separation between the projected energies of the two configurations is much smaller for the even spins than the odd ones at high spins, indicating much more sufficient configuration mixing in the even-spin band, i.e., the $n = 0$ band. This kind of configuration mixing is a reflection of the quasiparticle alignment.
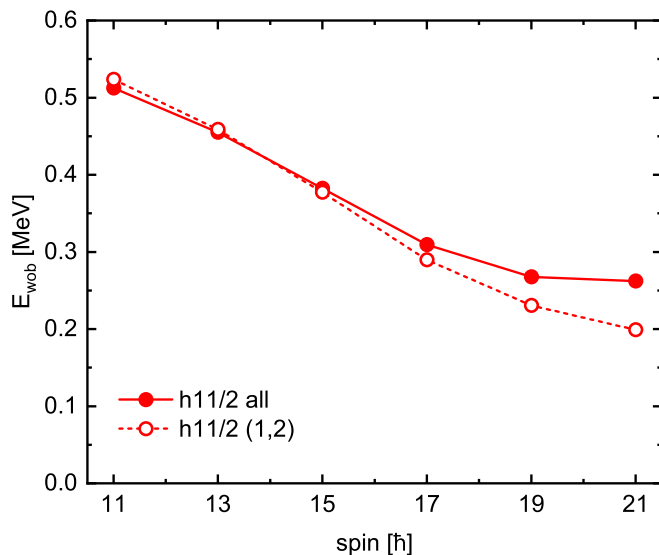
FIG. 8. The wobbling energies extracted according to Eq. (10) as functions of spin, calculated with and without configuration mixing. The solid line and solid symbols represent results calculated with the configuration mixing within the $\pi h_{11/2}$ subshell, while the dashed line and open symbols represent those calculated with the single configuration $h_{11/2}(1, 2)$.

The quasiparticle alignment has a suppression effect on the rotational energy, which can be, according to the above discussion, more pronounced for the $n = 0$ band. Therefore, one may conclude that the quasiparticle alignment tends to enlarge the energy separation between the $n = 1$ and $n = 0$ bands, i.e., to increase the wobbling energy extracted according to Eq. (10). This could be confirmed by comparing the wobbling energies calculated with and without quasiparticle alignment, which are shown in Fig. 8. It seems that the two factors destructing the transverse wobbling, i.e., the collective rotation around the i axis and the quasiparticle alignment, have opposite effects on the wobbling energy. The behavior of E_{wob} as the transverse wobbling collapses might be complex due to the combination of the above two opposite effects.

IV. SUMMARY

In this work the even- and odd-spin two-quasiparticle yrast bands in ^{136}Nd are investigated in a microscopic framework, i.e., the triaxial projected shell model, to see if they can be the $n = 0$ and $n = 1$ bands of transverse wobbling. The observed spectra are reasonably reproduced by a single diagonalization of the model Hamiltonian with the projected basis based on the self-consistent HFB minimum. The evolution of the orientation of the angular momentum vector with respect to the intrinsic frame tends to support a possible transverse wobbling interpretation close to the bandhead. The validity of the wobbling approximation, expressed in terms of the angular momentum related quantities, is examined quantitatively. The results suggest that the transverse wobbling is realized at the bandhead to a similar extent as the established transverse wobbler in ^{130}Ba, but gets destructed faster as spin increases, possibly due to the faster quasiparticle alignment as a result of its smaller deformation. It is noted that the effect of quasiparticle alignment is more pronounced in the $n = 0$ band than in the $n = 1$ one, as the energy separation between the s-axis-aligned configuration and the i-axis-aligned configuration is smaller for the even-spin band than for the odd-spin one, which, actually, can be connected to the decreasing behavior of the transverse wobbling energy. Such a distinction between the two bands tends to enlarge the wobbling energy, making its behavior at the collapse of transverse wobbling more complex than what is expected within the frozen alignment approximation.

[1] A. Bohr and B. R. Mottelson, *Nuclear Structure* (Benjamin, New York, 1975), Vol. II.

[2] E. R. Marshalek, Nucl. Phys. A **266**, 317 (1976).

[3] E. R. Marshalek, Nucl. Phys. A **275**, 416 (1977).

[4] I. N. Mikhailov and D. Janssen, Phys. Lett. B **72**, 303 (1978).

[5] D. Janssen and I. N. Mikhailov, Nucl. Phys. A **318**, 390 (1979).

[6] E. R. Marshalek, Nucl. Phys. A **331**, 429 (1979).

[7] S. Frauendorf and F. Dönau, Phys. Rev. C **89**, 014322 (2014).

[8] M. Matsuzaki, Y. R. Shimizu, and K. Matsuyanagi, Phys. Rev. C **65**, 041303(R) (2002).

[9] I. Hamamoto, Phys. Rev. C **65**, 044305 (2002).

[10] Y. R. Shimizu, M. Matsuzaki, and K. Matsuyanagi, arXiv:nucl-th/0404063.

[11] J. H. Hamilton, S. J. Zhu, Y. X. Luo, A. V. Ramayya, S. Frauendorf, J. O. Rasmussen, J. K. Hwang, S. H. Liu, G. M. Ter-Akopian, A. V. Daniel *et al.*, Nucl. Phys. A **834**, 28c (2010).

[12] Y. X. Luo, J. H. Hamiltonian, A. V. Ramayya, J. K. Hwang, S. H. Liu, J. O. Rasmussen, S. Frauendorf, G. M. Ter-Akopian, A. V. Daniel, and Y. T. Oganessian, in *Exotic Nuclei: Exon-2012: Proceedings of the International Symposium* (World Scientific, Singapore, 2013).

[13] N. V. Zamfir and R. F. Casten, Phys. Lett. B **260**, 265 (1991)

[14] P. Bringel, G. B. Hagemann, H. Hübel, A. Al-khatib, P. Bednarczyk, A. Bürger, D. Curien, G. Gangopadhyay, B. Herskind, D. R. Jensen *et al.*, Eur. Phys. J. A **24**, 167 (2005).

[15] S. W. Ødegård, G. B. Hagemann, D. R. Jensen, M. Bergström, B. Herskind, G. Sletten, S. Törmänen, J. N. Wilson, P. O. Tjøm,

I. Hamamoto, K. Spohr, H. Hubel, A. Görgen, G. Schönwasser, A. Bracco, S. Leoni, A. Maj, C. M. Petrache, P. Bednarczyk, and D. Curien, Phys. Rev. Lett. **86**, 5866 (2001).

[16] D. R. Jensen, G. B. Hagemann, I. Hamamoto, S. W. Ødegård, B. Herskind, G. Sletten, J. N. Wilson, K. Spohr, H. Hübel, P. Bringel, A. Neußer, G. Schönwaßer, A. K. Singh, W. C. Ma, H. Amro, A. Bracco, S. Leoni, G. Benzoni, A. Maj, C. M. Petrache, G. Lo Bianco, P. Bednarczyk, and D. Curien, Phys. Rev. Lett. **89**, 142503 (2002).

[17] G. Schönwaßer, H. Hübel, G. B. Hagemann, P. Bednarczyk, G. Benzoni, A. Bracco, P. Bringel, R. Chapman, D. Curien, J. Domscheit et al., Phys. Lett. B **552**, 9 (2003).

[18] H. Amro, W. C. Ma, G. B. Hagemann, R. M. Diamond, J. Domscheit, P. Fallon, A. Gorgen, B. Herskind, H. Hübel, D. R. Jensen et al., Phys. Lett. B **553**, 197 (2003).

[19] D. J. Hartley, R. V. F. Janssens, L. L. Riedinger, M. A. Riley, A. Aguilar, M. P. Carpenter, C. J. Chiara, P. Chowdhury, I. G. Darby, U. Garg et al., Phys. Rev. C **80**, 041304(R) (2009).

[20] I. Hamamoto and G. B. Hagemann, Phys. Rev. C **67**, 014319 (2003).

[21] J. Timár, Q. B. Chen, B. Kruzsicz, D. Sohler, I. Kuti, S. Q. Zhang, J. Meng, P. Joshi, R. Wadsworth, K. Starosta et al., Phys. Rev. Lett. **122**, 062501 (2019).

[22] J. T. Matta, U. Garg, W. Li, S. Frauendorf, A. D. Ayangeakaa, D. Patel, K. W. Schlax, R. Palit, S. Saha, J. Sethi et al., Phys. Rev. Lett. **114**, 082501 (2015).

[23] N. Sensharma, U. Garg, S. Zhu, A. D. Ayangeakaa, S. Frauendorf, W. Li, G. Bhat, J. A. Sheikh, M. P. Carpenter, Q. B. Chen et al., Phys. Lett. B **792**, 170 (2019).

[24] S. Nandi, G. Mukherjee, Q. B. Chen, S. Frauendorf, R. Banik, S. Bhattacharya, S. Dar, S. Bhattacharyya, C. Bhattacharya, S. Chatterjee, S. Das, S. Samanta, R. Raut, S. S. Ghugre, S. Rajbanshi, S. Ali, H. Pai, M. A. Asgar, S. Das Gupta, P. Chowdhury, and A. Goswami, Phys. Rev. Lett. **125**, 132501 (2020).

[25] C. M. Petrache, P. M. Walker, S. Guo, Q. B. Chen, S. Frauendorf, Y. X. Liu, R. A. Wyss, D. Mengoni, Y. H. Qiang, A. Astier et al., Phys. Lett. B **795**, 241 (2019).

[26] Q. B. Chen, S. Frauendorf, and C. M. Petrache, Phys. Rev. C **100**, 061301(R) (2019).

[27] Y. K. Wang, F. Q. Chen, and P. W. Zhao, Phys. Lett. B **802**, 135246 (2020).

[28] S. Biswas, R. Palit, U. Garg, G. H. Bhat, S. Frauendorf, W. Li, J. A. Sheikh, J. Sethi, S. Saha, P. Singh et al., Eur. Phys. J. A **55**, 159 (2019).

[29] N. Sensharma, U. Garg, Q. B. Chen, S. Frauendorf, D. P. Burdette, J. L. Cozzi, K. B. Howard, S. Zhu, M. P. Carpenter, P. Copp et al., Phys. Rev. Lett. **124**, 052501 (2020).

[30] S. Chakraborty, H. P. Sharma, S. S. Tiwary, C. Majumder, A. K. Gupta, P. Banerjee, S. Ganguly, S. Rai, Pragati, Mayank et al., Phys. Lett. B **811**, 135854 (2020).

[31] K. Tanabe and K. Sugawara-Tanabe, Phys. Rev. C **95**, 064315 (2017).

[32] S. Frauendorf, Phys. Rev. C **97**, 069801 (2018).

[33] K. Tanabe and K. Sugawara-Tanabe, Phys. Rev. C **97**, 069802 (2018).

[34] S. Guo, X. H. Zhou, C. M. Petrache et al., arXiv:2011.14354.

[35] M. Matsuzaki and S.-I. Ohtsubo, Phys. Rev. C **69**, 064317 (2004).

[36] E. A. Lawrie, O. Shirinda, and C. M. Petrache, Phys. Rev. C **101**, 034306 (2020).

[37] B. F. Lv, C. M. Petrache, A. Astier, E. Dupont, A. Lopez-Martens, P. T. Greenlees, H. Badran, T. Calverley, D. M. Cox, T. Grahn et al., Phys. Rev. C **98**, 044304 (2018).

[38] P. Ring and P. Schuck, The Nuclear Many-Body Problem (Springer-Verlag, Berlin, 1980).

[39] G. F. Bertsch and L. M. Robledo, Phys. Rev. Lett. **108**, 042505 (2012).

[40] Q.-L. Hu, Z.-C. Gao, and Y. S. Chen, Phys. Lett. B **734**, 162 (2014).

[41] K. Hara and Y. Sun, Int. J. Mod. Phys. E **4**, 637 (1995).

[42] Y. Sun, Phys. Scr. **91**, 043005 (2016).

[43] F. Q. Chen, Q. B. Chen, Y. A. Luo, J. Meng, and S. Q. Zhang, Phys. Rev. C **96**, 051303(R) (2017).

[44] F. Q. Chen, J. Meng, and S. Q. Zhang, Phys. Lett. B **785**, 211 (2018).

[45] Q. B. Chen and J. Meng, Phys. Rev. C **98**, 031303(R) (2018).

[46] E. Streck, Q. B. Chen, N. Kaiser, and U.-G. Meißner, Phys. Rev. C **98**, 044314 (2018).

[47] T. Bengtsson and I. Ragnarsson, Nucl. Phys. A **436**, 14 (1985).

[48] M. Baranger and K. Kumar, Nucl. Phys. A **110**, 490 (1968).

[49] http://www-phynu.cea.fr/science_en_ligne/carte_potentiels_microscopiques/carte_potentiel_nucleaire_eng.htm.